

Accepted Manuscript

Multi-scale progressive failure simulation of 3D woven composites under uniaxial tension

Gang Liu, Li Zhang, Licheng Guo, Feng Liao, Tao Zheng, Suyang Zhong

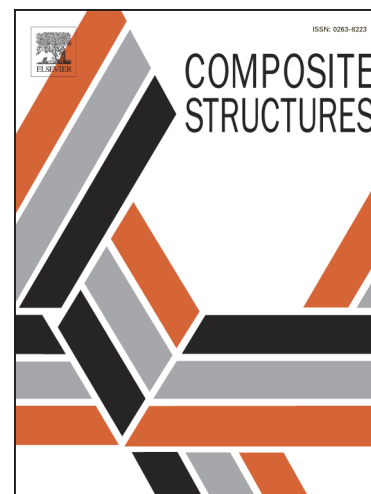
PII: S0263-8223(18)32024-5
DOI: <https://doi.org/10.1016/j.compstruct.2018.09.081>
Reference: COST 10228

To appear in: *Composite Structures*

Received Date: 4 June 2018
Revised Date: 11 September 2018
Accepted Date: 23 September 2018

Please cite this article as: Liu, G., Zhang, L., Guo, L., Liao, F., Zheng, T., Zhong, S., Multi-scale progressive failure simulation of 3D woven composites under uniaxial tension, *Composite Structures* (2018), doi: <https://doi.org/10.1016/j.compstruct.2018.09.081>

This is a PDF file of an unedited manuscript that has been accepted for publication. As a service to our customers we are providing this early version of the manuscript. The manuscript will undergo copyediting, typesetting, and review of the resulting proof before it is published in its final form. Please note that during the production process errors may be discovered which could affect the content, and all legal disclaimers that apply to the journal pertain.



Multi-scale progressive failure simulation of 3D woven composites under uniaxial tension

Gang Liu¹, Li Zhang¹, Licheng Guo^{1,*}, Feng Liao¹, Tao Zheng¹, Suyang Zhong²

(1, Department of Astronautic Science and Mechanics, Harbin Institute of Technology, Harbin, P.R. China

150001.

2, Institute of Fluid Physics, China Academy of Engineering Physics, Mianyang 621999, PR China.

* Corresponding author: Tel.: +86 45186413725; Fax: +86 45186413725. E-mail: guolc@hit.edu.cn)

Abstract

This paper presents a multi-scale progressive failure modeling scheme to analyze the damage behaviors of 3D angle-interlock woven composites under uniaxial tension. The macro-scale progressive damage model is established based on a meso-scale representative volume cell (RVC) model by using the inhomogeneous finite element method. In current model, a modified Puck criterion for fiber yarn and parabolic yield criterion for the matrix are chosen to be the damage initiation and propagation criteria, which can clearly describe the fiber breakage, inter-fiber fracture and matrix crack in the level of the fiber yarn and the matrix. The tensile effective elastic properties and the failure strength as well as the damage evolution process of this 3D woven composite are predicted. A series of uniaxial tensile tests are conducted to validate the macro-scale progressive damage model. Experimental and numerical results are compared and discussed.

Keywords

3D woven composites, multi-scale, inhomogeneous finite element, damage, uniaxial tensile.

Nomenclature

\mathbf{u} displacement vector	\mathbf{N} shape function matrix
\mathbf{a}^e nodal displacement vector	\mathbf{K} total stiffness matrix
\mathbf{Q} total nodal force vector	\mathbf{B} strain transfer matrix
\mathbf{D} material stiffness matrix	\mathbf{T} force vector
ϑ, φ angles between the local coordinate system of the fiber yarns and the global coordinate of the Material	
f, m fiber, matrix t, c tension, compression	

\aleph_f	spatial region of fiber yarns	\aleph_m	spatial region of the matrix
$\sigma_i, \epsilon_i (i = f, m)$	stress and strain of the fiber yarn and matrix	\tilde{D}_i	damage factor matrix
$S_i(d) (i = f, m)$	compliance matrices	d_m	damage variable of the matrix
$d_{f,i} (i = 1 - 6)$	damage variables of the fiber yarn		
$E_{f,i}, G_{f,ij}, \nu_{f,ij}$	young's moduli of fiber yarn in i direction, shear moduli and Poisson's ratios in ij plane		
E_m, ν_m	elastic modulus and Poisson's ratio of matrix		
$\phi_{m,L}, \phi_{f,N}$	loading functions of matrix and fiber yarns		
$r_{f,N}, r_{m,L}$	($N=1t, 1c, 2t, 2c, 3t, 3c; L = t, c$) damage threshold factors of fiber yarns and matrix		
$S_{m,c}, S_{m,t}$	compressive and tensile strengths of matrix	m_f	stress magnification factor
$S_{f,ic}, S_{f,it} (i = 1, 2, 3)$	compressive and tensile strengths of fiber yarn in i direction		
θ'	angle of the most dangerous plane in transverse direction of the fiber yarns		
I_1	the first invariant of the corresponding stress tensor		
J_2	the second invariant of the corresponding deviatoric stress tensor		
$A_M (A_{m,L}, A_{f,N})$	damage degradation parameters	G_M	the fracture energies
E_M, X_M	moduli and strengths of the component materials		
a	the characteristic length of the element	\tilde{T}	coordinate transformation matrix
$H_{ij} (i=1, 2, 3, j=1, 2, 3)$	elements in the matrix	J_1, J_2	planes in the full-scale model

1. Introduction

The 3D woven composite is a typical inhomogeneous material consists of reinforced fiber and matrix. It exhibits anisotropic properties as a whole although the reinforced fiber and matrix in component materials are considered as transversely isotropic and isotropic, respectively. The mechanical properties of fiber with high modulus and high strength have been brought into full play under the support of matrix. Compared with the conventional laminated composites, 3D woven composites have the prospect of long-term application in industrial fields like aeronautics, space and civil construction owing to their robust mechanical properties in the thickness direction, excellent damage tolerance and perfect impact resistance [1][2].

The microstructures of 3D woven composites are determined largely by the fiber architecture to the woven preform and weaving process as well as the consolidation process [3]. However, microstructural defects like distortion, abrasion and breakage of the yarns, voids and resin-rich areas are unintentionally produced during the manufacturing process of 3D woven composites that can seriously affect material performance. To predict and measure the mechanical properties of 3D woven composites accurately, extensive damage models and failure tests have been conducted and developed by researchers. In the 1980s, Tensile mechanical properties of 3D and laminated fabric Kevlar 49/epoxy composites are compared experimentally [4]. Then a binary model of textile

composites has been proposed to predict the elastic parameters and failure strength [5-6]. A stress analysis method and extracted a unit cell volume from 3D woven composites has been put forward after then [7]. Reference [8] developed a progressive failure model for laminated composites to predict the tensile strength of laminates with a circular hole, three damage parameters have been defined to represent degradation of the longitudinal modulus, transverse modulus and shear modulus, respectively. Three-cell model [9], analytical model [10], multiphase finite element model [11], multi-scale damage progression model [12] are proposed and constructed based on microstructure to predict tensile properties of 3D woven composites. Incompatible multivariable finite element method combined homogenization theory was used to calculate the mechanical properties of 3D braided composite [13]. Asymptotic expansion homogenization method is another widely used method to simulate the non-linear behavior of RVC models of 3D woven composites [14] [15]. Damage evolution models depended on the fracture energy of the yarn and matrix constituents, characteristic length of element and equivalence [16-18] are established to predict the mechanical properties of 3D braided and woven composites. Warren et al. [19] summarized an extensive experimental study of composites reinforced with three-dimensional woven preforms subjected to tensile, compressive and in-plane shear loading and examined three innovate 3D woven architectures.

Representative volume unit model is one of the most popular methods at present. Once the unit cell is chosen, the local stress field within the unit cell can be easily obtained. The local failure criterion of meso components and the meso-scopic damage evolution models can be introduced to decide whether material is damaged and simulate the whole damage evolution process. Tsai-Hill criterion [20], Tsai-Wu criterion [21], Hoffman criterion [22], Hashin criterion [23], Chang-Chang criteria [24] Puck criterion [25] and LaRC03 criterion [26] are commonly used failure criteria. Combined with finite element method, boundary element method, finite difference method, discrete element method and multi-scale method et al. The mechanical properties and the damage evolution process of 3D composites have been predicted in recent years [27-38].

In this paper, a macro-scale progressive damage model of is established based on a meso-scale RVC model by using the inhomogeneous finite element method (also called the multiphase finite element method [11, 39]). Modified Puck criterion [18] and parabolic yield criterion is chosen to be the damage initiation and propagation criteria. The tensile failure behavior of a type of 3D angle-

interlock woven composites are simulated. Typical uniaxial tensile tests are carried out to validate the accuracy of the predicted results. Considering the size of the RVC, a reasonable mesh size is chosen to balance the precision and time of calculation.

2. Method

2.1 Inhomogeneous finite element method

The 3D woven composite is composed of fiber yarns and matrix. The fiber yarn is formed by the fibers and relatively small amounts of permeated matrix. The fiber yarn is assumed to be transversely isotropic and the matrix is assumed to be isotropic. In finite element analysis, the irregularities of cross-sections and the complexity of the spatial orientations of the fiber yarns bring great challenges to a fine mesh. Therefore, most studies focused on RVC models. Few macro progressive damage models of 3D woven composites are reported. This work establishes a macro progressive damage model based on RVC model considering the fiber breakage, inter-fiber fracture and matrix crack using inhomogeneous finite element method.

The advantage of the inhomogeneous finite element method is that the finite element model can be easily established without considering the distribution of the material components. The material properties are determined by the location of the integration point in the calculation procedure instead. Namely, the fiber yarn and the matrix cannot necessary be distinguished when mesh. Thus the mechanical properties of the material components are considered and the number of meshes is controlled. The diagram of the element in inhomogeneous finite element method is described in Figure 1.

In the finite element calculation process, the continuum space is discretized at first, and then the appropriate shape function is constructed so that the displacement of each point in the continuum space can be expressed by the discretized node displacement and the shape function. The displacement of any point in a cell can be expressed as:

$$\mathbf{u} = \mathbf{N}\mathbf{a}^e \quad 2-1$$

Where $\mathbf{u} = [u(x, y, z), v(x, y, z), w(x, y, z)]^T$ is the displacement vector, $\mathbf{N} = [\mathbf{N}_1, \mathbf{N}_2, \dots, \mathbf{N}_n]$ is the shape function matrix, $\mathbf{a}^e = [\mathbf{a}_1, \mathbf{a}_2, \dots, \mathbf{a}_n]^T$ is the nodal displacement vector.

The finite element solving equation of elastic problem can be expressed as:

$$\mathbf{K}\mathbf{a} = \mathbf{Q} \quad 2-2$$

Where $\mathbf{K} = \sum_e \mathbf{K}^e$ and $\mathbf{Q} = \sum_e \mathbf{Q}^e$ are the total stiffness matrix and nodal force vector, respectively, and the expression of \mathbf{K} and \mathbf{Q} are as follows:

$$\begin{cases} \mathbf{K}^e = \int_{V_e} \mathbf{B}^T \mathbf{D} \mathbf{B} dV \\ \mathbf{Q}^e = \int_{S_e} \mathbf{N}^T \mathbf{T} dV \end{cases} \quad 2-3$$

Where \mathbf{B} is the strain transfer matrix, \mathbf{D} is the material stiffness matrix and \mathbf{T} is the force vector.

It should be noted that \mathbf{D} is a function of the coordinate geometric location:

$$\mathbf{D} = \mathbf{D}(x, y, z) = \begin{cases} \mathbf{D}_{f, (\vartheta, \varphi)}(x, y, z) & \text{if } (x, y, z) \in \mathfrak{K}_f \\ \mathbf{D}_m(x, y, z) & \text{if } (x, y, z) \in \mathfrak{K}_m \end{cases} \quad 2-4$$

Which means if the integration point is in the yarn volume, the material property matrix $\mathbf{D}_{f, (\vartheta, \varphi)}(x, y, z)$ is chosen, otherwise $\mathbf{D}_m(x, y, z)$ is taken. ϑ and φ are the angles between the local coordinate system of the fiber yarns and the global coordinate system of the material. \mathfrak{K}_f and \mathfrak{K}_m denote the spatial regions of fiber yarns and the matrix, respectively.

To realize the above scheme, a program module of location judgment is proposed and introduced to the ABAQUS VUMAT subroutine by using the 3D nonlinear programming theory [40]. A space region of fiber yarn and matrix is surrounded by N space plans is assumed in this program module.

Then the integration points in this space satisfy:

$$g_i(x, y, z) \leq 0, i = 1, 2, \dots, N \quad 2-5$$

Where $g_i(x, y, z) = 0$ is the equation of i th space surface. $g_i(x, y, z) = 0$ and $-g_i(x, y, z) \leq 0$ represent the same surface. While $g_i(x, y, z) \leq 0$ and $-g_i(x, y, z) \leq 0$ represent two regions on both sides of this surface. For 3D woven composites, the following points should be observed during the process of programming the location determination module: 1) the whole material structure can be duplicated and superposed by a RVC. 2) the judging sequence of component material is from warp/weft yarns to binder yarns, then to matrix. 3) warp and weft yarns are parallel to one coordinate axis of global coordinate system of the structure, while a binder yarn should be described individually since it can be divided into multiple sections according to the angles between them and the global coordinate system. Figure 2. shows the structure and fiber orientation of a type of 3D woven composites.

2.2 Progressive damage criteria

To better describe the fiber breakage, inter-fiber fracture and matrix crack in the level of the fiber yarn and the matrix, a modified Puck criterion for fiber yarn and parabolic yield criterion for the

The fiber yarn and the matrix exhibit different failure modes under tensile and compressive stress conditions, damage variables of the matrix and the fiber yarn can be expressed as

$$\begin{cases} \mathbf{d}_m = \begin{cases} \mathbf{d}_{m,t} & \text{if } I_1 \geq 0 \\ \mathbf{d}_{m,c} & \text{if } I_1 < 0 \end{cases} \\ \mathbf{d}_{f,1} = \begin{cases} \mathbf{d}_{f,1t} & \text{if } \tilde{\sigma}_{f,11} \geq 0 \\ \mathbf{d}_{f,1c} & \text{if } \tilde{\sigma}_{f,11} < 0 \end{cases} \\ \mathbf{d}_{f,i} = \begin{cases} \mathbf{d}_{f,it} & \text{if } \tilde{\sigma}_{f,n} \geq 0 \\ \mathbf{d}_{f,ic} & \text{if } \tilde{\sigma}_{f,n} < 0 \end{cases} \quad (i = 2, 3) \end{cases} \quad 2-12$$

The damage initiation and evolution criteria of matrix and fiber yarn are defined as:

$$F_{m,L} = \Phi_{m,L} - r_{m,L} \leq 0, L = \{t, c\} \quad 2-13$$

$$F_{f,N} = \Phi_{f,N} - r_{f,N} \leq 0, N = \{1t, 1c, 2t, 2c, 3t, 3c\} \quad 2-14$$

Where $\Phi_{m,L}$ and $\Phi_{f,N}$ are the loading functions of matrix and fiber yarns. According to the Puck criteria and the parabolic yield criteria [43], they can be expressed as:

$$\begin{cases} \Phi_{m,t} = \frac{3J_2 + I_1(S_{m,c} - S_{m,t})}{S_{m,c}S_{m,t}} \text{ if } I_1 \geq 0 \\ \Phi_{m,c} = -\frac{3J_2 + I_1(S_{m,c} - S_{m,t})}{S_{m,c}S_{m,t}} \text{ if } I_1 < 0 \end{cases} \quad 2-15$$

$$\begin{cases} \Phi_{f,1t} = \frac{\varepsilon_{f,11}E_{f1} + m_f(v_{f,12}\tilde{\sigma}_{f,22} + v_{f,13}\tilde{\sigma}_{f,33})}{S_{f,1t}} \text{ if } \tilde{\sigma}_{f,11} \geq 0 \\ \Phi_{f,1c} = -\frac{\varepsilon_{f,11}E_{f1} + m_f(v_{f,12}\tilde{\sigma}_{f,22} + v_{f,13}\tilde{\sigma}_{f,33})}{S_{f,1c}} \text{ if } \tilde{\sigma}_{f,11} < 0 \end{cases} \quad 2-16$$

$$\begin{cases} \Phi_{f,2t} = \sin^2 \theta' + \cos^2 \theta' \Phi_{f,t}^{\max}(\theta') \\ \Phi_{f,3t} = \cos^2 \theta' + \sin^2 \theta' \Phi_{f,t}^{\max}(\theta') \end{cases} \text{ if } \tilde{\sigma}_{f,n} \geq 0 \quad 2-17$$

$$\begin{cases} \Phi_{f,2c} = \sin^2 \theta' + \cos^2 \theta' \Phi_{f,c}^{\max}(\theta') \\ \Phi_{f,3c} = \cos^2 \theta' + \sin^2 \theta' \Phi_{f,c}^{\max}(\theta') \end{cases} \text{ if } \tilde{\sigma}_{f,n} < 0 \quad 2-18$$

Where $S_{m,c}$ and $S_{m,t}$ are compressive and tensile strengths of matrix, $S_{f,ic}$ and $S_{f,it}$ ($i=1, 2, 3$) are the compressive and tensile strengths of fiber yarns in i direction. m_f is the ‘stress magnification effect’ caused by different moduli of fiber yarns and matrix. θ' denotes the angle of the most dangerous plane in transverse direction of the fiber yarns. Detailed expressions of $\Phi_{f,c}^{\max}(\theta')$ and $\Phi_{f,t}^{\max}(\theta')$ are provided in eference [18]. I_1 is the first invariant of the corresponding stress tensor, and J_2 are the second invariant of the corresponding deviatoric stress tensor. They can be written as:

$$\begin{cases} I_1 = \tilde{\sigma}_{m,11} + \tilde{\sigma}_{m,22} + \tilde{\sigma}_{m,33} \\ J_2 = \frac{1}{6}[(\tilde{\sigma}_{m,11} - \tilde{\sigma}_{m,22})^2 + (\tilde{\sigma}_{m,22} - \tilde{\sigma}_{m,33})^2 + (\tilde{\sigma}_{m,33} - \tilde{\sigma}_{m,11})^2] \end{cases} \quad 2-19$$

2.3 Damage evolution model

From our previous research on experiment, we found the failure mode is close to brittle failure. Thus the damage evolution model can be defined as exponential damage evolution law (figure 3):

$$d_{m,L} = 1 - \frac{1}{r_{m,L}} \exp [A_{m,L}(1 - r_{m,L})], L = \{t, c\} \quad 2-20$$

$$d_{f,N} = 1 - \frac{1}{r_{f,N}} \exp [A_{f,N}(1 - r_{f,N})], N = \{1t, 1c, 2t, 2c, 3t, 3c\} \quad 2-21$$

$$\begin{cases} d_{f,4} = d_{f,1} + d_{f,2} - d_{f,1}d_{f,2} \\ d_{f,5} = d_{f,2} + d_{f,3} - d_{f,2}d_{f,3} \\ d_{f,6} = d_{f,3} + d_{f,1} - d_{f,3}d_{f,1} \end{cases} \quad 2-22$$

Where $A_{m,L}$ and $A_{f,N}$ are the damage degradation parameters, detailed solving process can be find in appendix of reference [42]. The damage evolution law used in this paper considers the simple case of that proposed in reference [42]. The analytical solutions of parameters A_M can be obtained by Eq. 2-23

$$A_M = \frac{2a * X_M}{2E_M * G_M - 2a * X_M} \quad 2-23$$

Where A_M represents $A_{m,L}$ and $A_{f,N}$, E_M and X_M are the moduli and strengths of the component materials, respectively. G_M are the fracture energies, a is the characteristic length of the element. In this paper, a represents the mesh size of the element since all elements are cubic.

The description of the progressive model is conducted in the local coordinate system of fiber yarns. Thus in the finite element calculation, the relationship of the global coordinate system and the local coordinate system should be established. The coordinate transformation matrix \tilde{T} is used to correlate the stresses and strains of fiber yarns in these two coordinate systems. \tilde{T} can be written as:

$$\tilde{T} = \begin{bmatrix} H_{11}^2 & H_{21}^2 & H_{31}^2 & H_{11}H_{21} & H_{21}H_{31} & H_{31}H_{11} \\ H_{12}^2 & H_{22}^2 & H_{32}^2 & H_{12}H_{22} & H_{22}H_{32} & H_{32}H_{12} \\ H_{13}^2 & H_{23}^2 & H_{33}^2 & H_{13}H_{23} & H_{23}H_{33} & H_{33}H_{13} \\ H_{11}H_{12} & H_{21}H_{22} & H_{31}H_{32} & H_{11}H_{22} & H_{21}H_{32} & H_{31}H_{12} \\ H_{12}H_{13} & H_{22}H_{23} & H_{32}H_{33} & H_{12}H_{23} & H_{22}H_{33} & H_{32}H_{13} \\ H_{13}H_{11} & H_{23}H_{21} & H_{33}H_{31} & H_{13}H_{21} & H_{23}H_{31} & H_{33}H_{11} \end{bmatrix} \quad 2-24$$

Where $H_{ij}(i=1, 2, 3, j=1, 2, 3)$ is the elements in the matrix H :

$$H = \begin{bmatrix} \cos \vartheta & \sin \vartheta \cos \varphi & \sin \vartheta \sin \varphi \\ -\sin \vartheta & \cos \vartheta \cos \varphi & \cos \vartheta \sin \varphi \\ 0 & -\sin \varphi & \cos \varphi \end{bmatrix} \quad 2-25$$

Where the angles ϑ and φ are Euler angles.

3. Model

3.1 RVC model

The geometric RVC model of a type of 3D angle-interlock woven carbon/epoxy composites is obtained by normalizing the statistics of the cross-sections and the fiber yarn orientations based on the cubic spline implementation method. This kind of composite consists of 12K T700 carbon fibers for the warp and weft yarns, 3K T300 carbon fibers for the binder yarns and TDE-86 resin for the matrix. Determination process of the RVC model is shown in figure 4. Statistical data suggests that the cross-section areas of weft/warp yarns and binder yarn are approximately 1.1 mm² and 0.275 mm², respectively. For modeling and calculation convenience, a simplified octagonal cross-section is designed. The dimensions of the cross-section and the RVC model are shown in figure 5. Final dimensions of RVC is 6.6 mm * 6.6mm * 0.6 mm. The Fiber volume fraction is 50.9%, which is the same to the actual 3D composite material.

Spatial location equations of warp, weft and binder yarns in the RVC model can be easily acquired by 3D nonlinear programming.

3.2 Full-scale model

To investigate the macroscopic damage behavior of the 3D woven composites, a full-scale progressive damage model is established based on the actual testing specimen. The scheme of mesh and boundary conditions are given in figure 7.

Dimensions of the model is 120 mm * 20 mm * 5 mm, uniform cube elements are applied, the mesh size is 0.25 mm. The 8-nodes reduced integration element (C3D8R) is used in this model, the total number of DOFs is 2454543. The selection of boundary conditions plays a vital role in the simulation results. According to the actual force conditions of the specimen, the displacement value in X direction of plane J_1 is set as zero, point A in Plane J_1 is fixed. An appropriate displacement load (2.76mm) is applied on the plane J_2 , displacement values of point B in Y and Z directions are set as zeros (Figure 7). The structure of this kind of 3D woven composite can be regarded as duplication and arrangement of a certain number of the RVC.

The inhomogeneous finite element based multi-scale progressive failure model is implemented into a user-defined material subroutine VUMAT in ABAQUS. Calculation process of the program is shown in figure 8.

4. Results

4.1 Uniaxial tensile test

Mechanical properties of component materials are listed in table 1. This uniaxial tensile test is conducted by referencing the standard ASTM D5379 on Zwick Z100 testing machine. Three specimens are tested and dimensions of the specimen and the experimental setups are shown in figure 6. Strain gages and extensometer are used simultaneously to record the history of strains when specimens subject to uniaxial tensile loading with a speed of 0.5 mm per minute. The size of the specimen is 250 mm * 20 mm * 5 mm, four aluminum tabs are bonded to the ends of a specimen on both sides. Thus the effective length of the specimen is 120 mm.

4.2 Results and discussions

Figure 9 compares the stress-strain relationships between experiment and numerical simulation under uniaxial tensile load. Strains measured by extensometer are chosen as the final strains considering the data stability and the mesostructure of the 3D woven composite. From the full-scale model, the average stress data is obtained by dividing the reaction force at the fixed end by the cross-sectional area. Calculated moduli and strengths of this kind of 3D woven composite material are listed in table 2. Both the numerically predicted and experimental measured longitudinal moduli are determined by computing the slope of initial linear stage of the stress-strain curves over a strain range of 0.23% - 0.35% since no damage occurs. The simulated curves are almost linear before failure, when damage occurs, it expands rapidly and reaches damage threshold. This is consistent with the brittle fracture phenomenon observed in experimental process. Averaged moduli and strengths of experimental results are 52.701GPa and 900.773 MPa, respectively, and simulated results of those are 54.053GPa and 973.561MPa, respectively. The stiffness and strength errors of the experimental and simulated results are 2.57% and 8.08%, respectively. From the values in table 2 and curves in figure 9, we find that simulated stress-strain curve correlate with the experimental ones very closely. The brittle failure occurs at the strain range of 1.70%-1.80%. From experimental results we know that this kind of material exhibits brittle fracture. The stress-strain response is approximate to linear relationship, but not completely linear since damage occurs before failure. The slope of simulated stress-strain response to damage changes gradually, but not that obviously. In this model, the slope of the stress-strain curves decreases from 54.681 to 51.559.

Diagram of distinguishing the fiber yarns and matrix in the 3D woven composites specimen depending on the locations of the integration points is shown in figure 10, different colors represent different material components, red represents the matrix, yellow represents the binder yarns, light blue represents the warp yarns, navy blue represents the weft yarns. According to the real structure of tested specimen in figure 4, there are eight layers of warp yarns, nine layers of weft yarns and eight layers of binder yarns, the distance between two parallel yarns is 3.3 mm. All this structural features can be accurately and effectively described by the proposed model in figure 10. Namely, the correctness of the location determination module program is validated.

Figure 11 shows the damage initiation and accumulation of the damage variables warp yarns ($d_{f,1}$) and weft yarns ($d_{f,2}$ and $d_{f,3}$) under tensile load. Notably, damage accumulation of the damage variable of matrix (d_m) is the similar to that of the weft yarns. This is because the inter-fiber fracture will occur in weft yarns when applying uniaxial load in warp direction. While the inter-fiber fracture is essentially the matrix crack since the fiber yarn is formed by the fibers and relatively small amounts of permeated matrix. As shown in Figure 11, damage initiates in matrix first, damage related to $d_{f,2}$ in weft yarns occurs when strain is in the range of (0.54% - 0.94%). Then slight damage related to $d_{f,1}$ occurs around the strain of 1.15%. During the strain range of 1.15% - 1.79%, damage related to $d_{f,2}$ expands rapidly, while damage related to $d_{f,1}$ and $d_{f,3}$ increase slowly. When strain reaches around 1.80%, damage related to $d_{f,1}$ expands rapidly and the warp fibers breakage result in the failure of the whole structure. Figure 11(a1, a2, a3), (b1, b2, b3) and (c1, c2, c3) show the damage accumulation related to $d_{f,1}$, $d_{f,2}$, and $d_{f,3}$ at the strains of 0.73%, 1.37% and 1.80%, respectively.

For experimental study, initial damage first occurs in matrix on the surface of the specimen, the matrix particles detach gradually when the load increase. Then the specimen is accompanied by a series of crisp sound then the load reaches a certain value. This might be the damage occurs within several fiber yarns. When the load reached the ultimate value, the specimen fails instantaneously. The failure modes observed after experiment are shown in figure 12. Fiber yarn tensile breakage and pull-out is observed in figure 12(a) and 12(b). Matrix crack is shown in figure 12(c) and the inter-fiber fracture is observed by the electron microscope in figure 12(d).

The above analysis shows that the simulated macroscale progressive failure process correlate well with the specimen failure in experimental procedure, which validates the availability of the proposed

model.

Considering the size of the RVC as well as the computational efficiency, models with different mesh sizes are implemented using the FEM. The calculation results show that 0.25 mm is a reasonable mesh size that can balance the RVC size, the accuracy and efficiency of calculation.

5. Conclusion

A multi-scale progressive failure modeling scheme is presented to analyze the damage initiation and development of 3D angle-interlock woven composites under uniaxial tension load. The macroscale failure behaviors are simulated based on a RVC model by using inhomogeneous finite element method. Fiber yarn breakage, inter-fiber yarn fracture is predicted by using modified Puck criteria, the matrix crack is predicted by using the parabolic yield criterion.

Experimental results show that initial damage first occurs in matrix on the surface of the specimen, then the matrix particles detaches gradually with the increasing of the load. Finally, the brittle fracture occurs on the specimen along with the warp yarns breakage.

The proposed model is correlated and validated by experimental study. Simulated damage evolution and failure modes agrees well with that observe in experiment. Results show that damage initiates in matrix first and expands gradually when strain is in the range of (0.54% - 0.94%). Then slight damage related to $d_{f,1}$ occurs around the strain of 1.15%. When strain reaches around 1.80%, damage related to $d_{f,1}$ expands rapidly and the warp fibers breakage result in the failure of the whole structure. Additionally, models with different mesh sizes are simulated. The calculation results indicate that 0.25 mm is a reasonable mesh size.

In conclusion, the proposed model can predict the damage evolution progress of a full-size specimen with considering the fiber breakage, inter-fiber fracture and matrix crack.

References

- [1] Ha-Minh C, Imad A, Boussu F, et al. Experimental and numerical investigation of a 3D woven fabric subjected to a ballistic impact[J]. International Journal of Impact Engineering, 2016, 88(2005):91-101.
- [2] Li Z, Sun B, Gu B. FEM simulation of 3D angle-interlock woven composite under ballistic impact from unit cell approach[J]. Computational Materials Science, 2010, 49(1):171-183.

- [3] Tong L, Mouritz A P, Bannister M K. 3D fibre reinforced polymer composites [M]. Elsevier, 2002.
- [4] Guess T R, Reedy E D. Comparison of interlocked fabric and laminated fabric Kevlar 49/epoxy composites[J]. *Journal of Composites, Technology and Research*, 1985, 7(4): 136-142.
- [5] Cox B N, Carter W C, Fleck N A. A binary model of textile composites—I. Formulation[J]. *Acta metallurgica et materialia*, 1994, 42(10): 3463-3479.
- [6] Xu J, Cox B N, McGlockton M A, et al. A Binary Model of Textile Composites .2. The Elastic Regime[J]. *Acta Metallurgica et Materialia*, 1995(43): 3511-3524.
- [7] Nagai K, Yokoyama A, Maekawa Z, et al. The stress analysis method for three-dimensional composite materials[J]. *Applied Composite Materials*, 1994, 1(3): 197-216.
- [8] Tan S C. A progressive failure model for composite laminates containing openings[J]. *Journal of Composite Materials*, 1991, 25(5): 556-577.
- [9] Wu D L. Three-cell model and 5D braided structural composites[J]. *Composites Science and Technology*, 1996, 56(3): 225-233.
- [10] Gu B. Prediction of the uniaxial tensile curve of 4-step 3-dimensional braided preform[J]. *Composite structures*, 2004, 64(2): 235-241.
- [11] Zeng T, Wu L, Guo L. A finite element model for failure analysis of 3D braided composites[J]. *Materials Science and Engineering: A*, 2004, 366(1): 144-151.
- [12] Bahei-El-Din Y A, Rajendran A M, Zikry M A. A micromechanical model for damage progression in woven composite systems[J]. *International Journal of Solids and Structures*, 2004, 41(9-10): 2307-2330.
- [13] Sun H, Di S, Zhang N, et al. Micromechanics of braided composites via multivariable FEM[J]. *Computers & structures*, 2003, 81(20): 2021-2027.
- [14] Dong J, Feng M. Asymptotic expansion homogenization for simulating progressive damage of 3D braided composites[J]. *Composite Structures*, 2010, 92(4): 873-882.
- [15] Visroliia A, Meo M. Multiscale damage modelling of 3D weave composite by asymptotic homogenisation[J]. *Composite Structures*, 2013, 95: 105-113.
- [16] Guo-dong F, Jun L, Bao-lai W. Progressive damage and nonlinear analysis of 3D four-directional braided composites under unidirectional tension[J]. *Composite Structures*, 2009, 89(1): 126-133.

- [17] Zhang C, Xu X. Finite element analysis of 3D braided composites based on three unit-cells models[J]. *Composite Structures*, 2013, 98: 130-142.
- [18] Zhong S, Guo L, Lu H, et al. A continuum damage model for three-dimensional woven composites and finite element implementation[J]. *Composite Structures*, 2015, 128: 1-9.
- [19] Warren K C, Lopez-Anido R A, Goering J. Experimental investigation of three-dimensional woven composites[J]. *Composites Part A: Applied Science and Manufacturing*, 2015, 73: 242-259.
- [20] Hill R. A theory of the yielding and plastic flow of anisotropic metals[J]. *Proc. R. Soc. Lond. A*, 1948, 193(1033): 281-297.
- [21] Tsai S W, Wu E M. A general theory of strength for anisotropic materials[J]. *Journal of composite materials*, 1971, 5(1): 58-80.
- [22] Hoffman O. The brittle strength of orthotropic materials[J]. *Journal of Composite Materials*, 1967, 1(2): 200-206.
- [23] Hashin Z. Fatigue failure criteria for unidirectional fiber composites[J]. *Journal of Applied Mechanics*, 1981, 48(4): 846-852.
- [24] Chang F K, Chang K Y. A progressive damage model for laminated composites containing stress concentrations[J]. *Journal of composite materials*, 1987, 21(9): 834-855.
- [25] Puck A, Schürmann H. Failure analysis of FRP laminates by means of physically based phenomenological models[M]//*Failure Criteria in Fibre-Reinforced-Polymer Composites*. 2004: 832-876.
- [26] Davila C G, Camanho P P, Rose C A. Failure criteria for FRP laminates[J]. *Journal of Composite materials*, 2005, 39(4): 323-345.
- [27] Pinho S T, Darvizeh R, Robinson P, et al. Material and structural response of polymer-matrix fibre-reinforced composites[J]. *Journal of Composite Materials*, 2012, 46(19-20): 2313-2341.
- [28] Jia X, Xia Z, Gu B. Nonlinear viscoelastic multi-scale repetitive unit cell model of 3D woven composites with damage evolution[J]. *International Journal of Solids and Structures*, 2013, 50(22-23): 3539-3554.
- [29] Visrolia A, Meo M. Multiscale damage modelling of 3D weave composite by asymptotic homogenisation[J]. *Composite Structures*, 2013, 95: 105-113.
- [30] Zhong S, Guo L, Liu G, et al. A random waveness model for the stiffness and strength

- evaluation of 3D woven composites[J]. *Composite Structures*, 2016, 152: 1024-1032.
- [31] Dai S, Cunningham P R. Multi-scale damage modelling of 3D woven composites under uni-axial tension[J]. *Composite Structures*, 2016, 142: 298-312.
- [32] Saleh M N, Lubineau G, Potluri P, et al. Micro-mechanics based damage mechanics for 3D orthogonal woven composites: experiment and numerical modelling[J]. *Composite Structures*, 2016, 156: 115-124.
- [33] Zhang D, Chen L, Sun Y, et al. Meso-scale progressive damage of 3D five-directional braided composites under transverse compression[J]. *Journal of Composite Materials*, 2016, 50(24): 3345-3361.
- [34] Wan Y, Sun B, Gu B. Multi-scale structure modeling of damage behaviors of 3D orthogonal woven composite materials subject to quasi-static and high strain rate compressions[J]. *Mechanics of Materials*, 2016, 94: 1-25.
- [35] Reinoso J, Catalanotti G, Blázquez A, et al. A consistent anisotropic damage model for laminated fiber-reinforced composites using the 3D-version of the Puck failure criterion[J]. *International Journal of Solids and Structures*, 2017, 126: 37-53
- [36] Liu G, Zhang L, Guo L, et al. A modified V-notched beam test method for interlaminar shear behavior of 3D woven composites[J]. *Composite Structures*, 2017, 181: 46-57.
- [37] Ge J, He C, Liang J, et al. A coupled elastic-plastic damage model for the mechanical behavior of three-dimensional (3D) braided composites[J]. *Composites Science and Technology*, 2018, 157: 86-98.
- [38] Huang W, Zhang W, Chen T, et al. Dynamic response of circular composite laminates subjected to underwater impulsive loading[J]. *Composites Part A: Applied Science and Manufacturing*, 2018, 109: 63-74.
- [39] Zhai J, Zeng T, Xu G, et al. A multi-scale finite element method for failure analysis of three-dimensional braided composite structures[J]. *Composites Part B: Engineering*, 2017, 110: 476-486.
- [40] Durazzi C, Ruggiero V. Global Convergence of the Newton Interior-Point Method for Nonlinear Programming[J]. *Journal of Optimization Theory & Applications*, 2004, 120(1):199-208.
- [41] Lu H, Guo L, Liu G, et al. Progressive damage investigation of 2.5 D woven composites under

quasi-static tension[J]. *Acta Mechanica*, 2018: 1-14.

[42] Maimí P, Camanho P P, Mayugo J A, et al. A continuum damage model for composite laminates: Part II–Computational implementation and validation[J]. *Mechanics of Materials*, 2007, 39(10): 909-919.

[43] Catalanotti G, Camanho P P, Marques A T. Three-dimensional failure criteria for fiber-reinforced laminates[J]. *Composite Structures*, 2013, 95: 63-79.

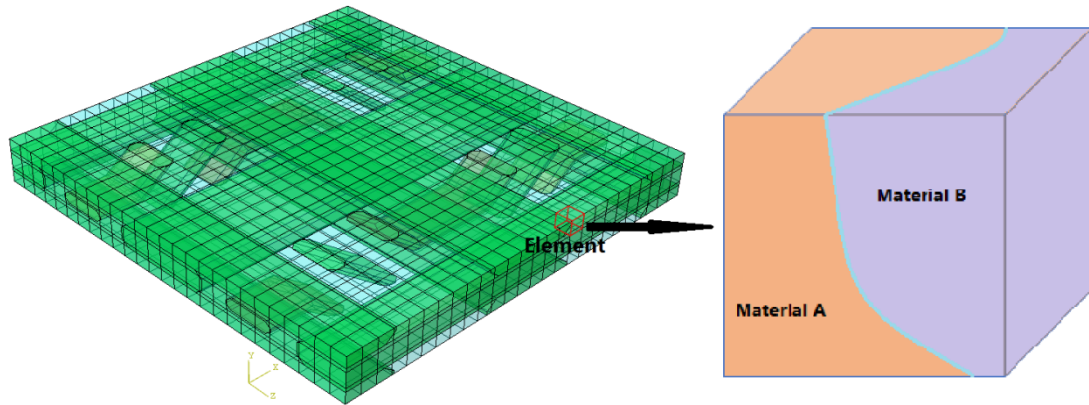


Figure 1. Element in inhomogeneous finite element method

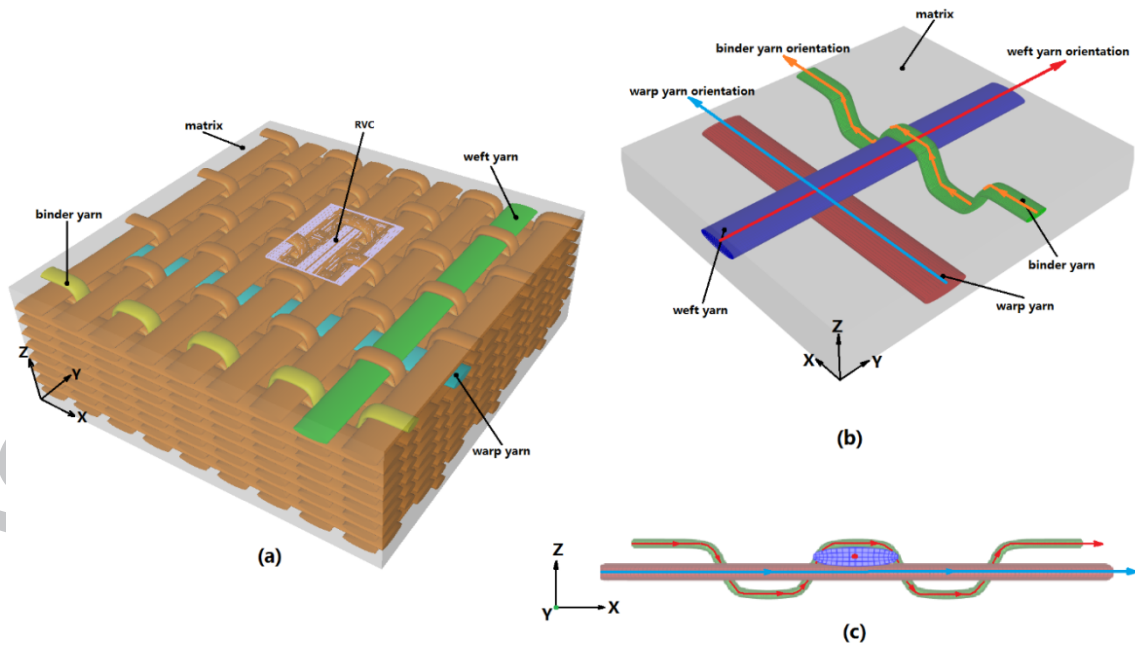


Figure 2. Structure and fiber orientation of 3D woven composites: (a) structure and RVC, (b) fiber orientation, (c) fiber orientation view along X-axis direction

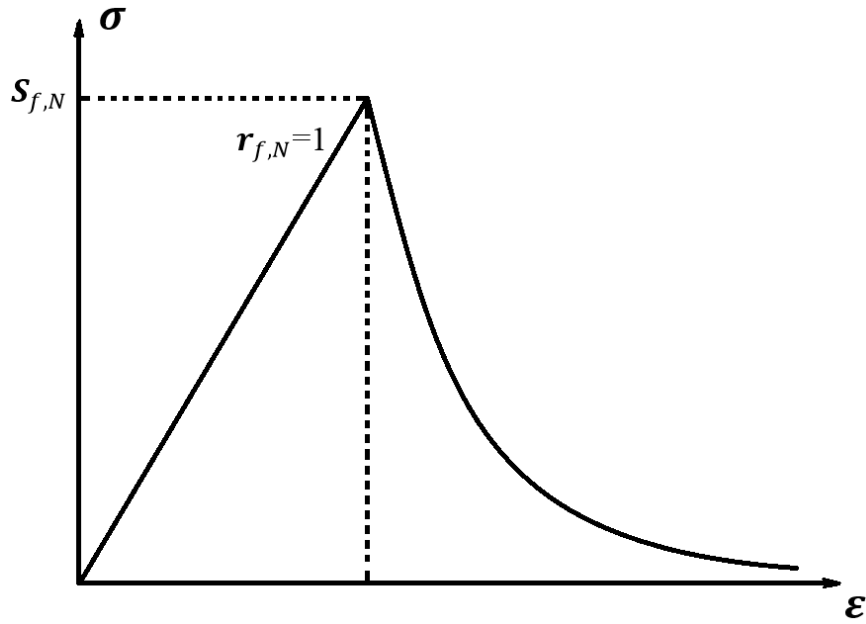


Figure 3. Scheme of the exponential damage evolution law

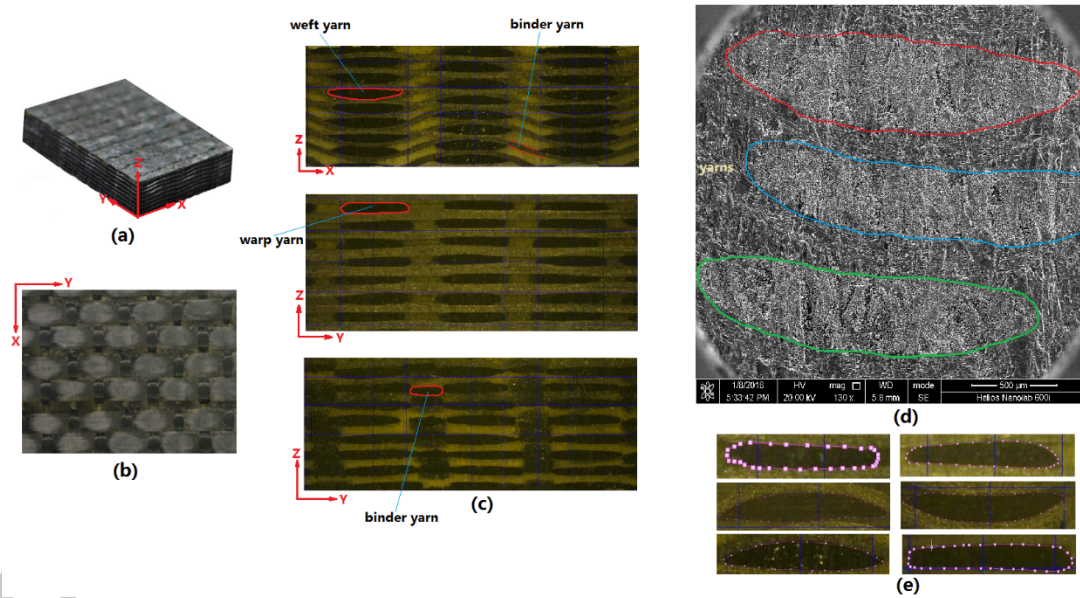


Figure 4. Determination process of the RVC: (a) appearance [16] (b) surface of 3D composites, (c) cross-sections in different directions, (d) micro-yarns by SEM, (e) statistical cross-sections

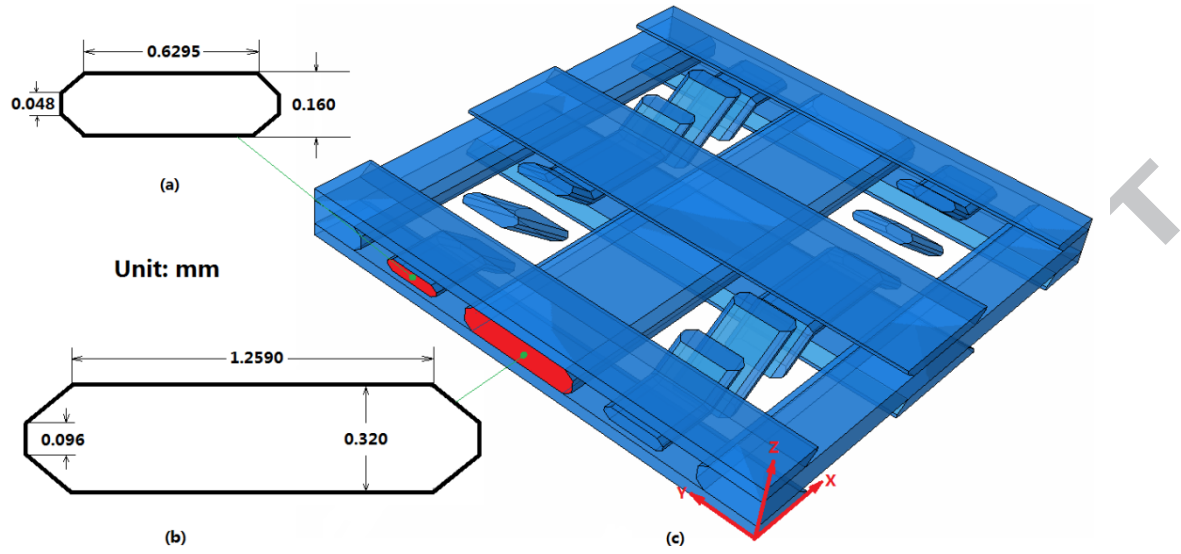


Figure 5. Simplified geometric model: (a) cross-section of binder yarn, (b) cross-section of warp/weft yarn, (c) RVC model

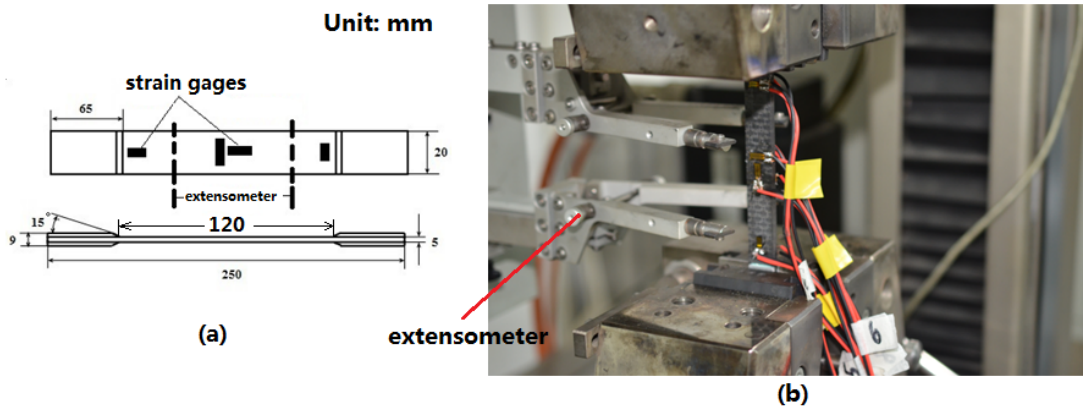


Figure 6. Experiment: (a) specimen, (b) setups

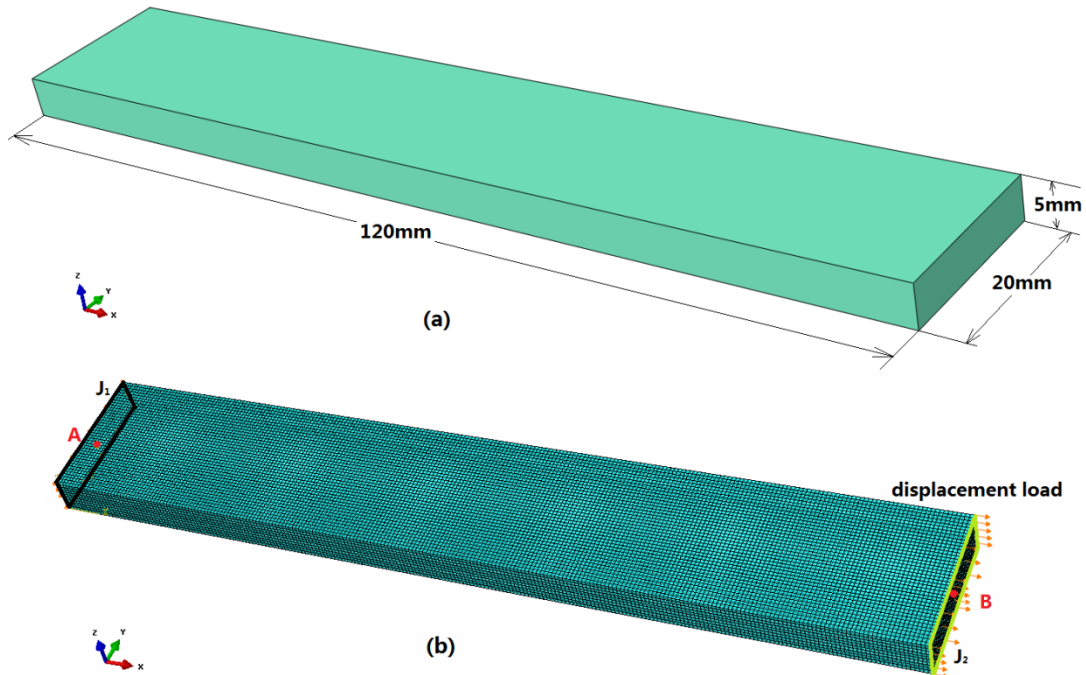


Figure 7. Scheme of mesh and boundary conditions: (a) dimensions, (b) boundary conditions

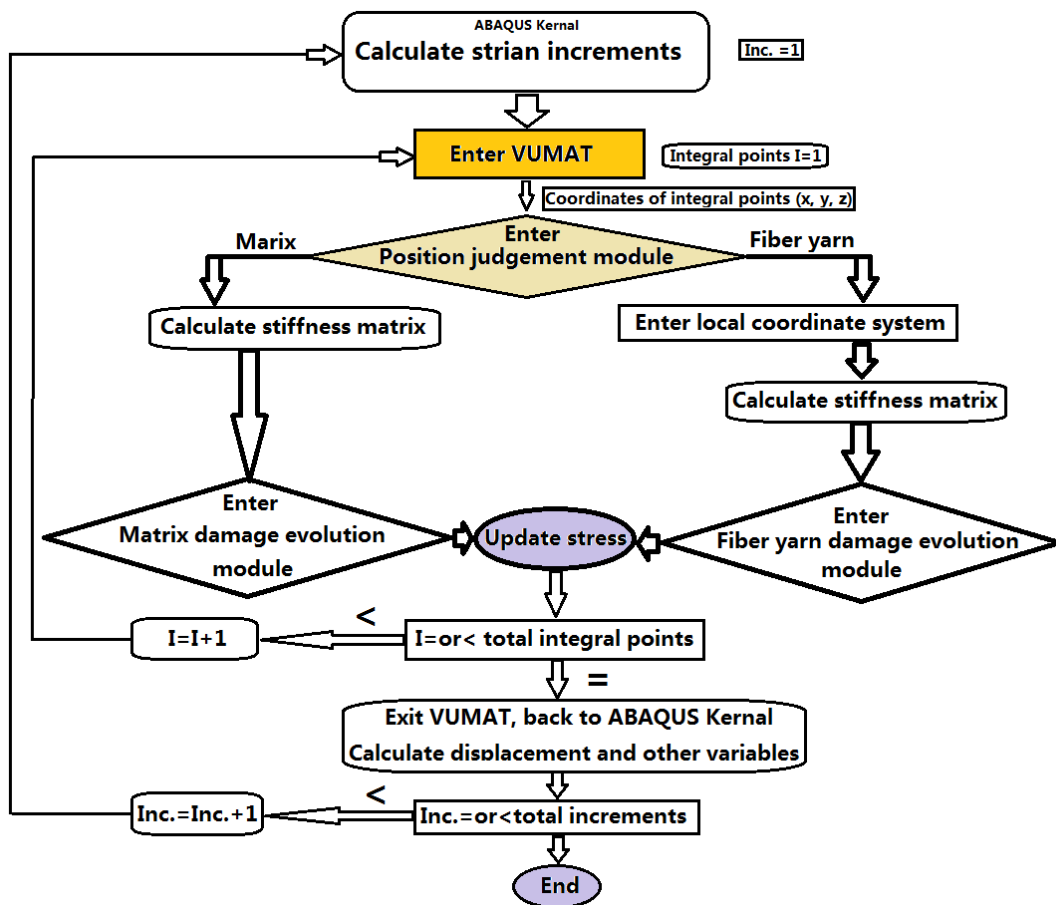


Figure 8. Scheme of calculation process

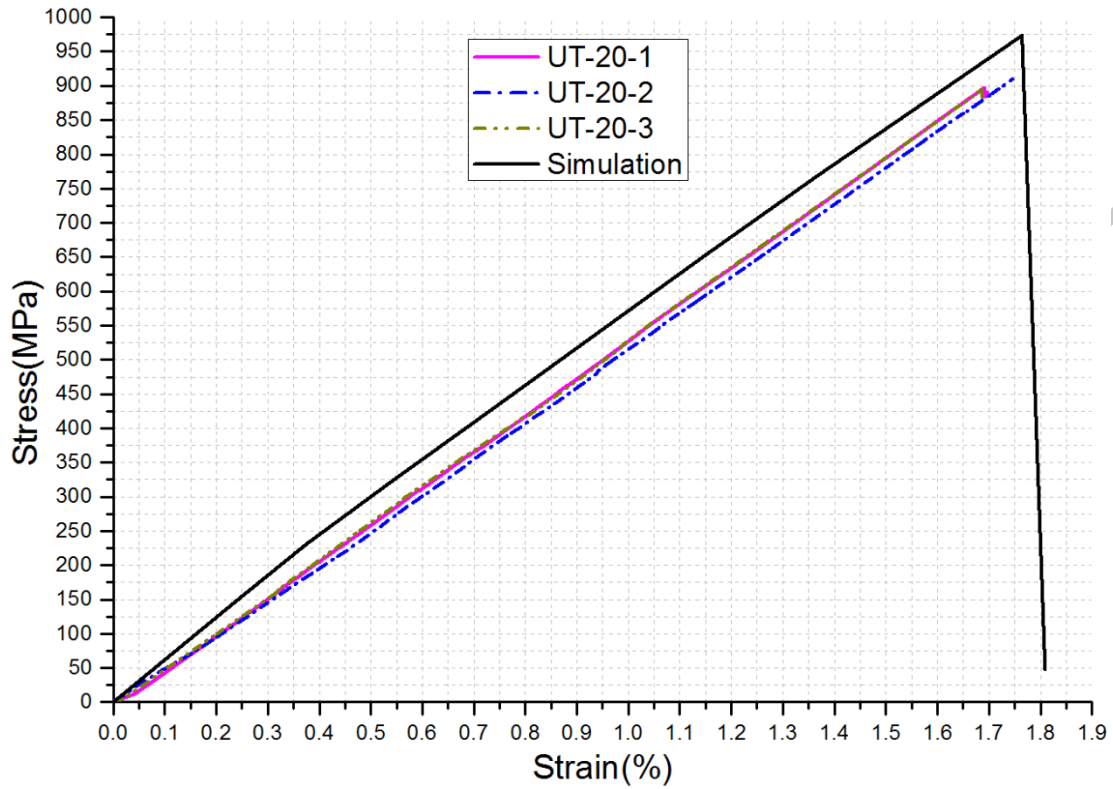


Figure 9. Comparison of stress-strain curves between simulation and experiment

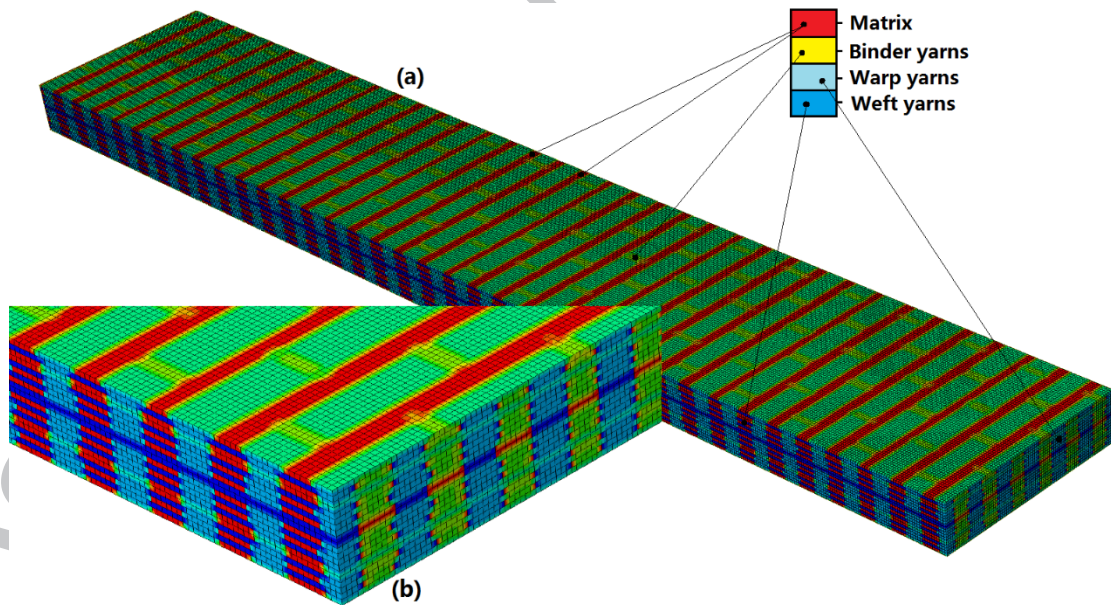


Figure 10. Locations of fiber yarns and matrix: (a) the whole specimen, (b) detail view

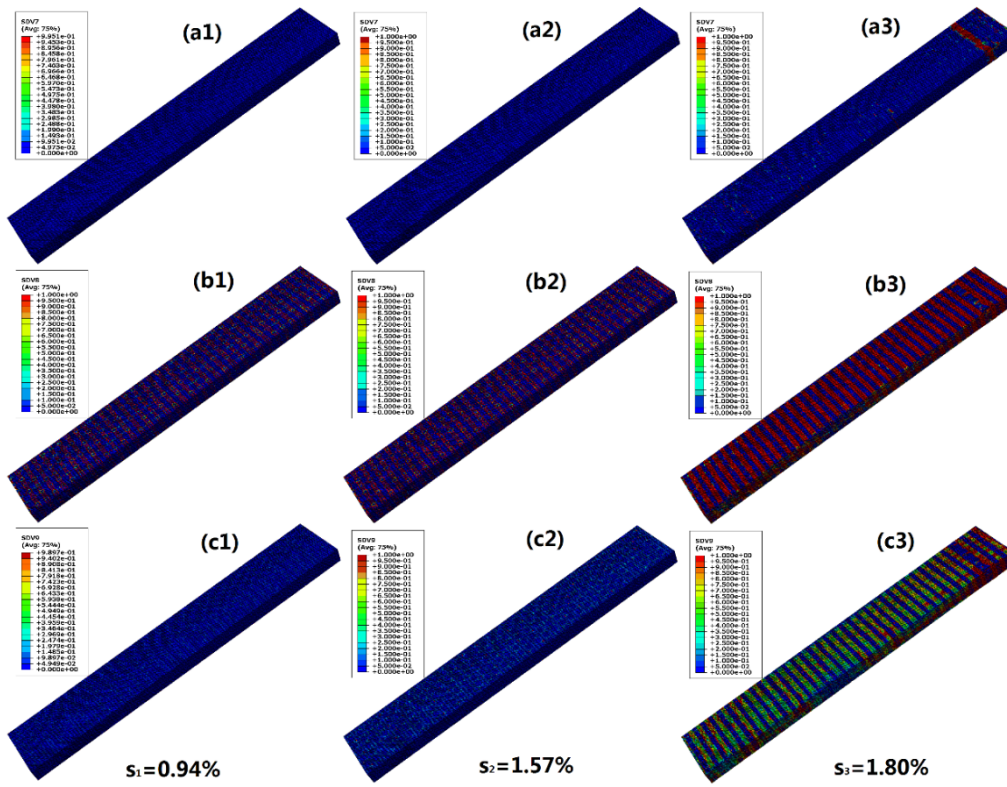


Figure 11. Damage initiation and accumulation of the damage variables: (a1, a2, a3) $d_{f,1}$, (b1, b2, b3) $d_{f,2}$ and d_m , (c1, c2, c3) $d_{f,3}$

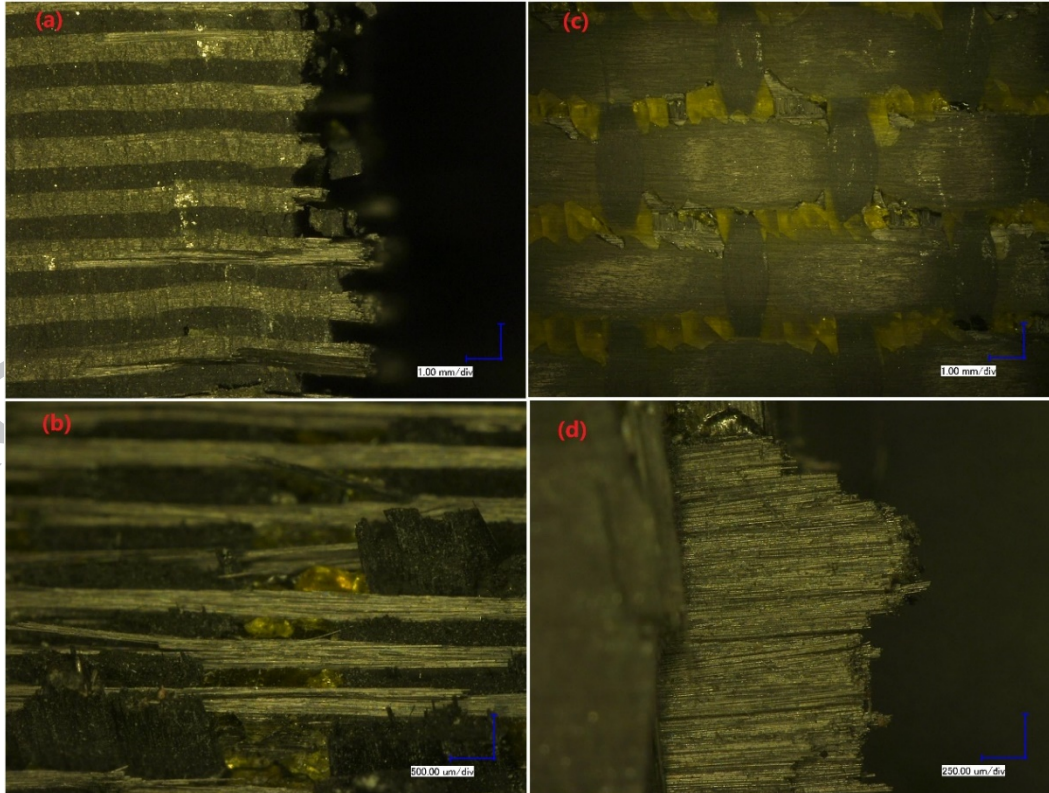


Figure 12. Experimental failure modes: (a) and (b) fiber yarn breakage, (c) matrix crack, (d) inter-fiber yarn fracture

Table 1. Mechanical properties of component materials [16]

	$E_{f,1}$	$E_{f,2}$	$G_{f,12}$	$\nu_{f,12}$	$\nu_{f,23}$	$S_{f,1t}$	Density
T700	230 GPa	18.2 GPa	36.6 GPa	0.27	0.3	4.9 GPa	1.80g/cm ³
T300	221 GPa	13.8 GPa	9.0 GPa	0.20	0.25	3.53 GPa	1.75g/cm ³
	E_m		ν_m		$S_{m,t}$		Density
TDE-86	3.55 GPa		0.33		241 GPa		1.22g/cm ³

Table 2. Calculated moduli and strengths of experimental and numerical results

	Specimen	Moduli (GPa)	Strengths(MPa)
Experiment	UT-20-1	53.583	897.410
	UT-20-2	53.103	909.976
	UT-20-3	51.416	894.933
	Average	52.701	900.773
Simulation	-	54.053	973.561
Error (%)	-	2.57	8.08

ACCEPTED